Brodogradnja Volume 75 Number 4 (2024) 75402

journal homepage: www.brodogradnja.fsb.hr

Brodogradnja

An International Journal of Naval Architecture and Ocean Engineering for Research and Development

Novel approaches to representing the speed–time characteristics of a direct start-up induction machine driving gravitational-type loads

Ilija Knežević[1], Tatijana Dlabač[1], Martin Ćalasan[2], Maja Krčum[3]*

Affiliation
[1] *Faculty of Maritime Studies Kotor, University of Montenegro*
[2] *Faculty of Electrical Engineering, University of Montenegro*
[3] *Faculty of Maritime Studies, University of Split*

ARTICLE INFO

Editor-in-Chief: Prof. Nastia Degiuli
Associate Editor: PhD Ivana Martić

Keywords:
Mathematical modeling
Gravitational loads
Induction machine
Ship auxiliary machines
Ship's power system

ABSTRACT

On ships, practically all types of induction machine loads are present, among which those with fan and gravitational characteristics are the most common. This paper addresses the speed–time curve dependency on the direct start of an induction machine under gravitational load. The characteristic of speed–time, $\omega = f(t)$, is described through two analytical expressions. The first expression is derived using the formula for torque based on Thévenin's equivalent circuit, while the second expression is derived from Kloss's formula for torque. The mathematical model has been tested through simulation and experimental validation on an induction machine in laboratory conditions. Also, the paper includes a realised MATLAB program for determining the mentioned characteristics. The results show the high precision and practical applicability of the proposed analytical expressions in different working conditions.

1. Introduction

The development of electrical systems on ships began in the 1880s when the ship "Columbia" was equipped with a direct current (DC) power source, which was used for lighting [1,2]. However, a true revolution in marine electrical energy occurred through discoveries such as the induction machine (IM), the transformer and the diesel engine at the end of the 19th century and beginning of the 20th [3]. These discoveries spurred additional research and development, directing the shipbuilding industry towards more advanced and complex electrical systems that have become standard on today's ships [4]. In this context, IMs have emerged as one of the most significant devices on ships. Specifically, IMs are alternating-current rotary machines, which are most commonly used as motors and generators on ships [5]. The primary advantage of these machines lies in their robustness, efficiency and ability to provide consistently high performance under various operational conditions [6]. Although IMs require increased torque during start-up, their basic design

* Corresponding author.
E-mail address: tanjav@ucg.ac.me

http://dx.doi.org/10.21278/brod75402
Submitted 14.02.2024; Accepted 25.07.2024.
ISSN 0007-215X; eISSN 1845-5859

and reliability make them crucial for maritime applications, particularly during manoeuvring [7,8] and for many other operations [9].

Regardless of its size or purpose, every ship relies on a reliable electrical power network (EPN) to function smoothly [10]. Technological advancement has increased the demand for electrical power on ships [11]. Modern ships contain advanced navigation systems, communication equipment, air-conditioning units and many other electrical devices that require a stable power supply [12]. The ship's EPN represents a complex assembly that includes various voltage levels [13].

Electric motor drives on a ship can be compared to those used on land. Both types consist of an electric motor, a working mechanism, a connecting element, a control part and a network connection [14]. However, there are several specificities for ship IMs compared to those intended for use on land [6]. These specificities include a particular class of insulation, protection against sea salt and moisture, increased resistance to vibrations and the ability to withstand swaying, certain inclinations and similar conditions [3,15]. In the context of ships' electric motor drives, the key characteristics that determine their operational performance are the starting torque and starting current [16,17]. These characteristics are of great importance because they determine the speed and efficiency with which the motor transitions from a state of rest to a working state, as well as the impact of the start on the overall electrical power network of the ship [18]. In addition to these technical aspects, integrated control systems serve for the efficient management, monitoring of consumption, diagnostics and optimisation of the entire ship's EPN [19].

IMs, which are crucial for operating ship auxiliary devices, are characterised by specific loads that are essential for their efficient operation [13,16]. Specific loads of IMs found on ships include fan, gravitational, and linear loads. For fan loads, the torque is a quadratic function of speed; for linear loads, the torque is a linear function of speed; while for gravitational loads, the torque is constant and does not depend on speed. One of the most prominent loads on a ship is the gravitational load, which is typical for auxiliary ship machines and devices that generate a constant torque load [12]. This group includes various types of ships' winches, cranes, elevators, compressors and similar devices. When a ship's auxiliary machine has the ability to return mechanical energy to the IM, thus switching the machine from motor to generator mode, we can then speak about a potential torque load [3]. In practice, when an IM drives a ship's crane or elevator, it works in either the first or second quadrant on the ω–M plane, where the speed varies while the torque load does not change sign.

Electric motor drives represent the largest group of energy consumers on a ship, accounting for approximately 75%–80% of the total generated electrical energy, with IMs being the most common [3,12]. Their significant application in electric propulsion systems, where some motors can be connected to high voltage directly or via transformers, underscores their importance [10]. However, the initiation of these motors is especially critical; during start-up, the current drawn from the electrical network can be 6–8 times higher than the nominal current, potentially destabilising the ship's EPN and affecting the stability and quality of the electrical supply [18,20]. As such, understanding and managing the starting process of IMs is paramount. Namely, for the stability of the power system, it is important to reduce the current during the start of the motor. Thus, different starting methods have been developed, such as direct online [21], star-delta switches [22,23], autotransformers [24], soft starters [25] and inverters [26]. For high-power IMs, the substantial moments of inertia can lead to insulation damage if the starting time exceeds the machine's short-circuit withstand time. The starting time of an IM can be determined through three basic approaches: numerical techniques; graphical methods; and analytical solutions.

The first approach, based on numerical techniques, is used in Numerical Time-Domain Computation (NTDC) [27]. This approach uses a series of differential equations to describe the dynamic behaviour of the IM. Once these equations are formulated, numerical integration methods (namely the classic Euler's method, the well-known Runge–Kutta method, or the Finite Element Method) are utilised to solve them. Software tools such as MATLAB/Simulink, Ansys, or similar, based on these methods, enable simulation of the starting times of IMs [28]. However, it should be noted that this approach is computationally demanding, especially for complex models.

Graphical methods provide a visual analysis of starting time through speed–torque curves. These curves of the torque of the IM and the driven load are presented on a standard graph, which is then divided into segments. In each segment, the torque is interpolated and then all the values are summed up to obtain the total starting time [29].

The behavior of the IM, especially during the starting time, is shown by a mathematical model. In one of the studies, Aree [30] deals with calculating the starting times for medium- and high-voltage IMs and proposes an exact formula. He particularly highlights the accuracy of this approach when the machine is started using standard techniques. Building on the foundation of previous research, Ćalasan, along with his collaborators, has continued to explore the field of the start-up of IMs in his publications [28,31–34]. In paper [31], an invertible analytical formula is introduced for the mathematical modeling of the starting time of an IM under no-load conditions, utilising Kloss's expression for torque and solving it through the Lambert *W* equation. In another paper [28], using Thévenin's theorem for the calculation of the IM current as well as the torque, he derives an invertible analytical solution for calculating the no-load starting time of the motor. Additionally, paper [32] provides an analytical solution for the acceleration of the IM, as well as a methodology for determining its maximum value. In contrast to these approaches, paper [33] focuses on modeling the speed–time characteristics of IMs in no-load conditions, examining the losses due to friction in the bearings. In the context of a ship's electrical power system, where the IM often drives a fan-type load, the authors in paper [34] modeled direct starting under such load conditions. This method allows for precise calculation of the starting time of the IMs used in marine applications, such as pumps, fans and thrusters.

In this paper, a novel approach to mathematical modeling of the speed–time characteristic under gravitational (constant) load conditions is proposed. The primary outcomes and significant insights from this research are:

- This paper introduces novel and original mathematical expressions for the speed–time characteristics of modeling an IM that is directly started under gravitational load conditions. These expressions are based on Kloss's formula for torque and application of Thévenin's equivalent circuit for torque calculation.
- A software approach implementing the aforementioned mathematical modeling technique is presented.
- The results of simulations and experimental investigation of the proposed mathematical expressions are provided, confirming their applicability.
- The proposed expressions were tested for various machine power and voltage values, demonstrating their robustness in different operational conditions and wide applicability in practice.

This paper is organised into seven sections. The second section describes the ship's electric motor drive. The third section presents original and novel mathematical expressions for the speed–time characteristics of directly started IMs under a gravitational load. The fourth section focuses on software approaches to modeling the speed–time characteristics of IMs' gravitational-type loads. The fifth section pertains to simulation results that demonstrate the applicability and accuracy of the proposed expressions. The sixth section of the paper provides experimental verification of the proposed formulas. Finally, the seventh section summarises the essential findings and highlights potential directions for future research.

2. Shipboard Electrical Power Systems

The shipboard electrical power systems are based on the principle of a central plant for generating electrical energy, similar to that on land. These systems include several generators, which are mainly powered by diesel engines or steam turbines. These generators can be paralleled and synchronised on the main switchboard, supplying electrical power to all consumers on board [35]. Management of the generators is enabled through a Power Management System (PMS), which automatically switches generators on and off according to the current demand for electrical power. The standard frequency on board is typically 50/60 Hz. For three-phase voltage levels, the standard voltages are 380/440 V and 690/660 V, while single-phase

voltages are set at 240 V and 120 V. For alternating current systems, the upper limit for low voltage is 1000 V and for direct current systems, it is 1500 V [36,37].

For high-voltage systems, the standard voltages range from above 1 kV to 15 kV. Electrical distribution on ships is based on different systems for different voltage levels, namely for high-voltage and low-voltage levels. The distribution network can have a ring or radial configuration [12,37]. The main distribution board is divided into at least two segments to ensure redundancy in case of failures. It provides power supply to all consumers on board, including the power supply to the ship's auxiliary machines, which are crucial for the operation of the main ship's engine. The auxiliary machines on board, such as cranes, winches, pumps, fans, thrusters and compressors, are powered by the IM [3,38].

For the analysis and modeling of electromotive drive systems on ships, it is important to understand the operation of IMs and the load characteristics of a ship's auxiliary machines. As illustrated in Figure 1, the electromotive drive powering a ship's auxiliary machine has typical load characteristics, which can be categorised as: hyperbolic; linear; fan-type; and gravitational [34]. Auxiliary machines and devices on board can be divided into two main groups: those that typically rotate in one direction, such as fans, centrifuges, thrusters, reels and pumps (known as reactive loads); and those where the direction of rotation changes rapidly or slowly during the operating cycle, such as cranes, elevators and the like [34,39].

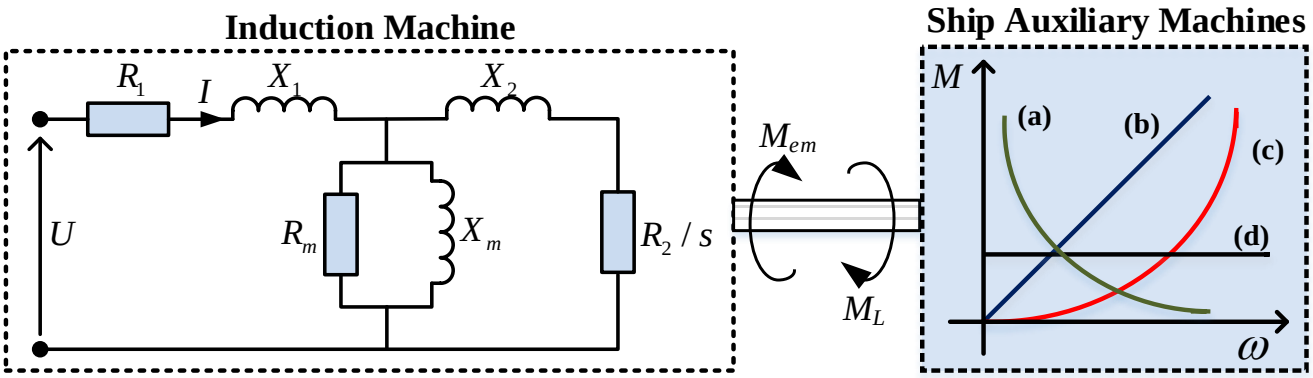

Fig. 1 Electromotive drive and stationary torque curves of a ship's auxiliary machines

(a) hyperbolic – $M_L = \frac{B}{\omega}$; (b) linear – $M_L = B\omega$; (c) fan – $M_L = B\omega^2$; (d) gravitational $M_L = B$

3. Novel approach to representing the speed–time curve for a gravitational type of load

It is important to emphasise that the derived analytical expressions presented below are valid only under the assumption that all the parameters of the IM are constant. This assumption simplifies the analysis but may not fully reflect the real operational conditions, where parameters can vary due to factors such as changes in temperature, slip, component wear and voltage fluctuations. Specifically, the application to IMs with more complex rotor designs, such as those with multiple cages or deep-bar rotors, can result in different torque and slip, which are not directly covered by these models.

To derive the expression for the starting time of an IM under gravitational load, Thévenin's equivalent circuit is used, as shown in Figure 2. This represents a simplified equivalent circuit derived from Figure 1. Here, U_T is the Thévenin voltage, representing the open-circuit voltage at the terminals of the network when the load is removed. X_T is the Thévenin reactance, representing the equivalent reactance seen by the load, and R_T is the Thévenin resistance, representing the equivalent resistance seen by the load. In this context, the rotor circuit is treated as the load. X_2 represents the rotor reactance, while R_2/s is the rotor resistance divided by the slip (s), which indicates the resistance experienced by the rotor as it decelerates from synchronous speed. This division by slip is crucial as it reflects the varying resistance seen by the rotor during different operational speeds.

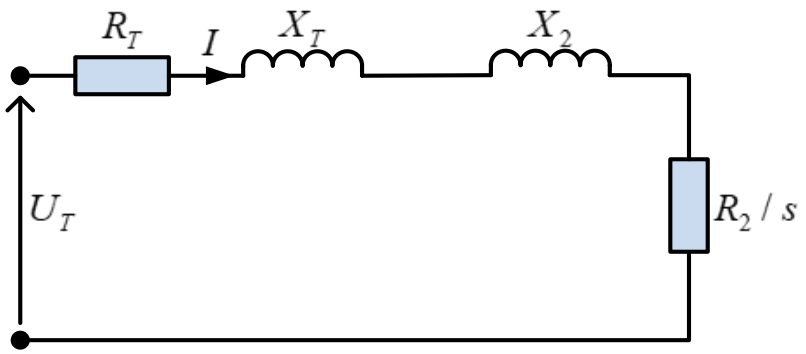

Fig. 2 Thévenin's equivalent circuit

The developed electromagnetic torque of an IM can be calculated using the well-known expressions for torque as follows:

$$M = \frac{3(U_T/\sqrt{3})^2}{\omega_s}\left(\frac{\frac{R_2}{s}}{\left(R_T+\frac{R_2}{s}\right)^2+\left(X_T+X_2\right)^2}\right) \tag{1}$$

where:

U_T is the value of the Thévenin voltage source ($U_T = \frac{X_m}{X_1+X_m}U$),

X_T is the value of the Thévenin reactance ($X_T = \frac{X_m R_1^2 + X_1^2 X_m + X_1 X_m^2}{R_1^2+\left(X_1+X_m\right)^2}$), and

R_T is the value of the Thévenin resistance $R_T = \frac{R_1 X_m^2}{R_1^2+\left(X_1+X_m\right)^2}$, while

ω_s is the synchronous speed of the rotating magnetic field within the air gap ($\omega_s = \frac{2\pi n_s}{60}$).

In the context of IMs, the concept of rotor slip (s) is important for understanding machine performance and operational efficiency. Rotor slip is defined as the difference in speed between the rotating magnetic field, established by the stator, and the actual speed of the rotor, ω. It is expressed as a percentage of the synchronous speed, ω_s. Mathematically, this can be expressed as:

$$s(\%) = \frac{\omega_s - \omega}{\omega_s}\cdot 100 \tag{2}$$

For an approximate calculation of torque, which gives the relationship as a function of slip, and for a known value of maximum torque and its corresponding slip at the maximum torque of the machine, Kloss's expression is used.

$$M = \frac{2M_{br}}{\frac{s}{s_{br}}+\frac{s_{br}}{s}} \tag{3}$$

where:

M_{br} is the value of the maximum torque ($M_{br} = \frac{3(U_T/\sqrt{3})^2}{\omega_s}\left(\frac{X_T+X_2}{\left(R_T+X_T+X_2\right)^2+\left(X_T+X_2\right)^2}\right)$) and

s_{br} is the value of the corresponding slip at the maximum machine torque ($s_{br} = \frac{R_2}{\sqrt{R_T{}^2 + (X_T + X_2)^2}}$).

The following subsections present the derivation of expressions for the start-up time of the IM. The first proposed expression is derived using the torque equation from Thévenin's equivalent circuit, while the second proposed expression is derived using Kloss's expression for torque. Although the final expression for the start-up time of the IM has the same mathematical formulation, they differ in their coefficients.

3.1 First expression

In the context of dynamic analysis of an IM, Newton's equation for rotational motion can be formulated as:

$$\begin{aligned} M_{em} - M_L &= J \frac{d\omega}{dt} \\ M_{em} - M_L &= J \frac{d\left((1-s)\omega_s\right)}{dt} \\ M_{em} - M_L &= -J\omega_s \frac{ds}{dt} \end{aligned} \tag{4}$$

It is important to note that slip (s) is variable as a function of time because it changes during the IM start-up process. The driving torque in an IM is the developed electromagnetic torque (M_{em}). External forces such as gravitational load also cause a load torque (M_L) on the motor shaft. The moment of inertia of the rotor (J) represents a measure of the resistance to changes in rotational speed.

Common to all types of loads is the use of expressions for electromagnetic torque, such as the Thévenin expression and the Kloss expression. However, when a specific load torque (gravitational, fan, linear, no-load) is introduced into M_L, a completely different model for the starting time of the IM is obtained. Observing Thévenin expression for machine torque, and gravitational type of load, the slip-time IM characteristics have the following form:

$$\left(\frac{3\left(U_T/\sqrt{3}\right)^2}{\omega_s} \left(\frac{\frac{R_2}{s}}{\left(R_T + \frac{R_2}{s}\right)^2 + \left(X_T + X_2\right)} \right) - B \right) = -J\omega_s \frac{ds}{dt} \tag{5}$$

By applying standard mathematical operations, the previous equation can be rewritten in the following form:

$$dt = \frac{\left(J\omega_s{}^2 R_T{}^2 + J\omega_s{}^2 \left(X_T + X_2\right)^2\right)s^2 + \left(2J\omega_s{}^2 R_2 R_T\right)s + J\omega_s{}^2 R_2 R_T}{\left(B\omega_s \left(X_T + X_2\right)^2 + B\omega_s R_T{}^2\right)s^2 - \left(3U_T{}^2 R_2 - 2B\omega_s R_2 R_T\right)s + B\omega_s R_2{}^2} ds \tag{6}$$

The total start-up time for a loaded IM with a gravitational load characteristic, when directly connected to the network, is obtained as follows:

$$t = \int_1^s \frac{\left(J\omega_s{}^2 R_T{}^2 + J\omega_s{}^2 \left(X_T + X_2\right)^2\right)s^2 + \left(2J\omega_s{}^2 R_2 R_T\right)s + J\omega_s{}^2 R_2 R_T}{\left(B\omega_s \left(X_T + X_2\right)^2 + B\omega_s R_T{}^2\right)s^2 - \left(3U_T{}^2 R_2 - 2B\omega_s R_2 R_T\right)s + B\omega_s R_2{}^2} ds \tag{7}$$

The previous equation can be written in the most general mathematical form as follows:

$$t = \int_{1}^{s} \frac{\alpha_1 s^2 + \alpha_2 s + \alpha_3}{\alpha_4 s^2 - \alpha_5 s + \alpha_6} ds \tag{8}$$

where:

$$\begin{aligned}
\alpha_1 &= J\omega_s{}^2 R_T{}^2 + J\omega_s{}^2 \left(X_T + X_2\right)^2; \\
\alpha_2 &= 2J\omega_s{}^2 R_2 R_T; \\
\alpha_3 &= J\omega_s{}^2 R_2 R_T; \\
\alpha_4 &= B\omega_s \left(X_T + X_2\right)^2 + B\omega_s R_T{}^2; \\
\alpha_5 &= 3U_T{}^2 R_2 - 2B\omega_s R_2 R_T; \\
\alpha_6 &= B\omega_s R_2{}^2;
\end{aligned} \tag{9}$$

To streamline the integration process, the following form is introduced as an intermediate variable in the equation below. This facilitates the necessary algebraic manipulation by simplifying the transformation of the equation. Due to the identical degrees of the polynomial in the integral equation, division is required, resulting in the equation taking the following form:

$$\frac{\alpha_1 s^2 + \alpha_2 s + \alpha_3}{\alpha_4 s^2 - \alpha_5 s + \alpha_6} = \frac{\alpha_1}{\alpha_4} \left[1 + \frac{\left(\frac{\alpha_2}{\alpha_1} + \frac{\alpha_5}{\alpha_4}\right) s + \frac{\alpha_3}{\alpha_1} + \frac{\alpha_6}{\alpha_4}}{s^2 - \frac{\alpha_5}{\alpha_4} s + \frac{\alpha_6}{\alpha_4}} \right] \tag{10}$$

This equation is solved by applying the decomposition method in the following form:

$$\frac{\left(\frac{\alpha_2}{\alpha_1} + \frac{\alpha_5}{\alpha_4}\right) s + \frac{\alpha_3}{\alpha_1} + \frac{\alpha_6}{\alpha_4}}{(s - s_1)(s - s_2)} = \frac{k_1}{(s - s_1)} + \frac{k_2}{(s - s_2)} \tag{11}$$

The coefficients s_1 and s_2, given in equation (11), represent the real roots of the equation. The coefficients k_1 and k_2 can be solved observing the following equation:

$$\begin{bmatrix} k_1 \\ k_2 \end{bmatrix} = \begin{bmatrix} 1 & 1 \\ -s_2 & -s_1 \end{bmatrix}^{-1} \begin{bmatrix} \frac{\alpha_2}{\alpha_1} + \frac{\alpha_5}{\alpha_4} \\ \frac{\alpha_3}{\alpha_1} + \frac{\alpha_6}{\alpha_4} \end{bmatrix} \tag{12}$$

After decomposing equation (10) and solving the system of linear equations shown in equation (12), we get the final expressions for the coefficients k_1 and k_2. The expressions for k_1 and k_2 are derived as follows:

$$\begin{bmatrix} k_1 \\ k_2 \end{bmatrix} = \begin{bmatrix} \frac{\alpha_1\alpha_6 + \alpha_3\alpha_4 + s_1(\alpha_1\alpha_5 + \alpha_4\alpha_4)}{\alpha_1\alpha_4(s_1 - s_2)} \\ \frac{\alpha_1\alpha_6 + \alpha_3\alpha_4 + s_2(\alpha_1\alpha_5 + \alpha_4\alpha_4)}{\alpha_1\alpha_4(s_1 - s_2)} \end{bmatrix} \tag{13}$$

Furthermore, by approaching the analysis of real roots of the quadratic equation that occurs in the decomposition process, expressions for s_1 and s_2 were derived. These roots of the quadratic equation are

significant for understanding the dynamic properties of the IM under various slips. The expressions for s_1 and s_2 are given in the following formula:

$$\begin{bmatrix} s_1 \\ s_2 \end{bmatrix} = \begin{bmatrix} \frac{\alpha_5}{\alpha_4} + \sqrt{\frac{1}{4}\left(\frac{\alpha_5}{\alpha_4}\right)^2 - \frac{\alpha_6}{\alpha_4}} \\ \frac{\alpha_5}{\alpha_4} - \sqrt{\frac{1}{4}\left(\frac{\alpha_5}{\alpha_4}\right)^2 - \frac{\alpha_6}{\alpha_4}} \end{bmatrix} \tag{14}$$

Therefore, the acceleration time of an IM can be calculated as follows:

$$t = \int_1^s \frac{\alpha_1}{\alpha_4}\left[1 + \frac{k_1}{(s-s_1)} + \frac{k_2}{(s-s_2)}\right] ds \tag{15}$$

Finally, the start-up time of an IM to a certain speed is obtained by integrating the above expression within the limits from s=1 to s:

$$t = \frac{\alpha_1}{\alpha_4}(s-1) + \frac{\alpha_1}{\alpha_4} k_1 \ln\left(\frac{s-s_1}{1-s_1}\right) + \frac{\alpha_1}{\alpha_4} k_2 \ln\left(\frac{s-s_2}{1-s_2}\right) \tag{16}$$

The analytical expression derived to describe the speed-time characteristics under a gravitational load of an IM is a new contribution to the theory of electric machines. This expression significantly differs from those found in works [28,31], which focus on the speed-time characteristics in no-load conditions. Additionally, a completely different mathematical relation for time is given when the IM drives a linear type load [33] or a fan type load [34].

The formula we previously derived for calculating the starting time of the IM under gravitational load can also be applied to calculate the starting time of the machine using soft starts. This is because soft start involves a gradual increase in the supply voltage. Therefore, the formula we derived earlier can be used to calculate the time during each interval when the supply voltage remains constant.

3.2 Second expression

The speed–time characteristics can also be determined by utilising Kloss's equation for torque, allowing us to present the equation as follows:

$$\frac{2M_{br}}{\frac{s}{s_{br}} + \frac{s_{br}}{s}} - B = -J\omega_s \frac{ds}{dt} \tag{17}$$

Kloss's expression, derived from the Thévenin model, assumes that we neglect the stator resistance, which allows one to focus on the dominant effects of rotor slip in the analysis of machine torque. The previously mentioned equation (17), after a series of mathematical operations, can be transformed and displayed in the form defined by equation (8). In this case coefficient $\alpha_2 = 0$ while others have the following values:

$$\begin{aligned}
\alpha_1 &= J\omega_s;\\
\alpha_2 &= 0;\\
\alpha_3 &= J\omega_s {s_{br}}^2;\\
\alpha_4 &= B;\\
\alpha_5 &= 2M_{br}s_{br};\\
\alpha_6 &= B{s_{br}}^2;
\end{aligned} \tag{18}$$

4. A software approach to representing the speed–time curve for gravitational-type loads

The MATLAB/Simulink dynamic model of an IM driving a gravitational type of load during direct start and speed loading is presented in Figure 3. The detailed core segment of the developed MATLAB code, grounded on the equations above, is given in the APPENDIX. This section introduces a software-based methodology for determining the speed–time curve of an IM under gravitational loading, incorporating a series of mathematical steps. In the next section of the paper, the presented simulation results are aimed at testing the proposed mathematical equations describing the speed–time characteristics.

For building the IM model in the Simulink environment, the Simscape Electrical toolbox from MATLAB was used, specifically the SI Units Induction Machine block. This block enables precise modeling and simulation of the dynamic behaviour of the IM. The mathematical model behind this block includes a fourth-order state-space model for the electrical part of the machine, and a second-order system for the mechanical part. All electrical variables and parameters are referenced to the stator and expressed in an arbitrary two-axis reference frame (*dq* frame). The stator and rotor voltage equations describe the voltage–current relationships, the flux linkage equations define the relationships between the currents and fluxes in the stator and rotor, the electromagnetic torque equation determines the torque developed in the motor, and the mechanical dynamics equation describes the angular acceleration of the rotor, taking into account inertia and friction. To solve these equations, the NTDC method was used in the Simulink environment, using integrators to calculate the state variables over time.

For modeling the speed–time curve for the gravitational-type of loading on the ship, a software approach is proposed that includes a series of mathematical steps. The steps shown in Figure 4 illustrate the precise starting time calculation of a direct start-up IM when starting a gravitational-type load.

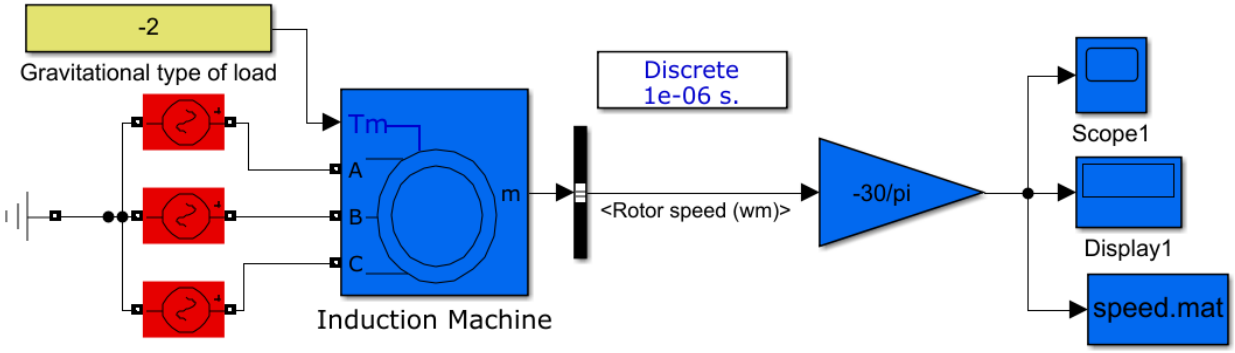

Fig. 3 MATLAB/Simulink dynamic model of an IM driving a gravitational type of load during direct start and speed loading

The software approach presented in the paper relies on MATLAB code and begins with setting the parameters of the IM. For modeling the speed–time characteristics, Thévenin's expression for torque is used, where coefficients are taken from relation (9). If the calculation is performed through another approach based on Kloss's expression for torque, the coefficients defined by relation (18) are taken. Further steps of the software approach include finding the roots s_1 and s_2, given in equation (14). Using a matrix (12), the coefficients k_1 and k_2 are determined, and then, utilising the expression for time (16), the speed–time characteristic of the IM is obtained.

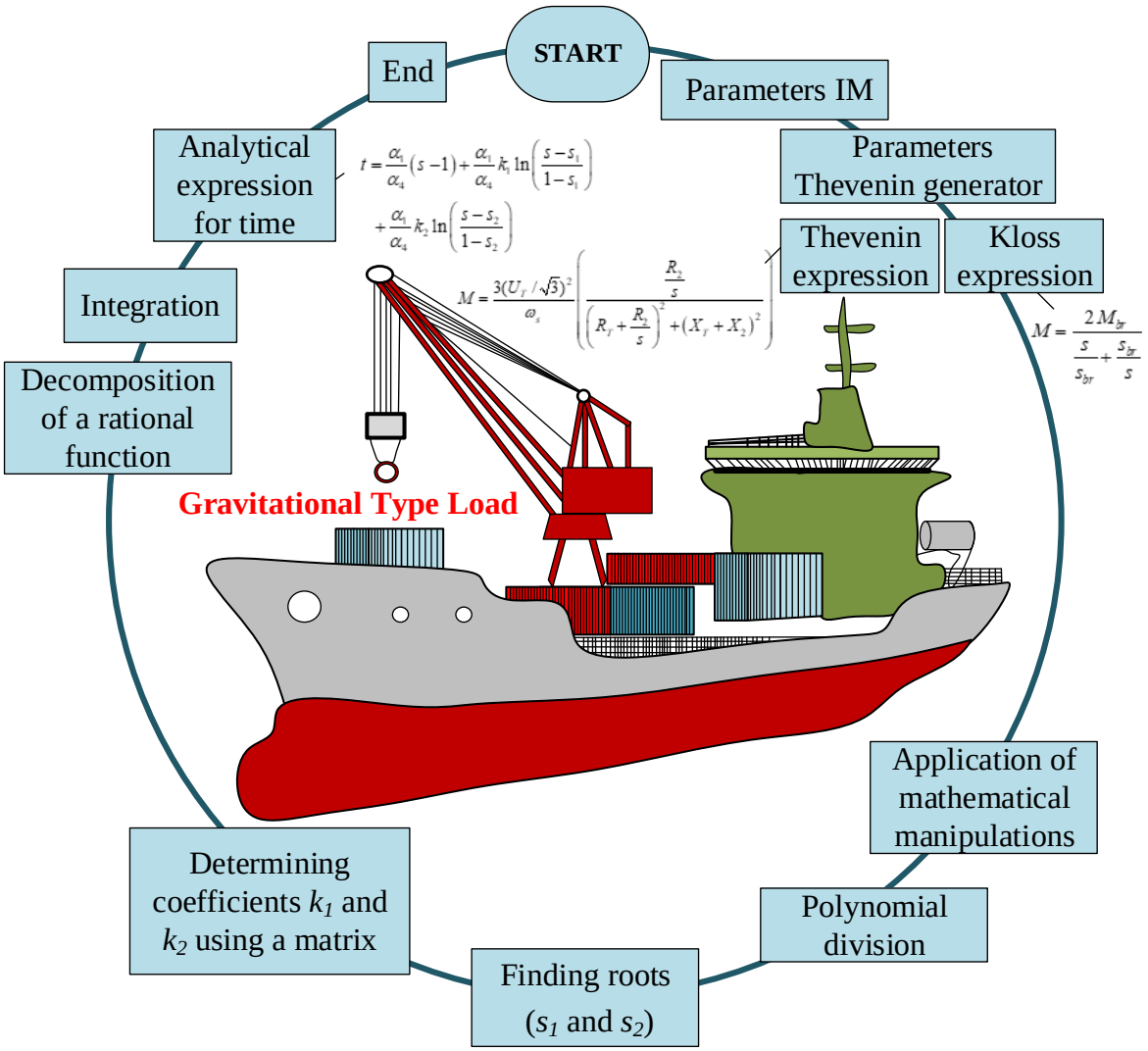

Fig. 4 Steps in modeling the speed–time characteristic for a gravitational load

5. Simulation results

In this section, the simulation results for IM under various operating scenarios are present. The goal of this investigation is to test the proposed mathematical equations for modeling the speed–time characteristics. For this purpose, Table 1 provides the parameters of the equivalent circuit of the IM used for simulation tests.

Table 1 Parameters of the IM used for the simulation

IM parameters [28]	***Value***
P_n [W]	3730
U [V]	575
f [Hz]	60
R_1 [Ω]	2.053
R_2 [Ω]	1.904
X_1 [Ω]	2.545
X_2 [Ω]	2.545
X_m [Ω]	98.77
J [kgm^2]	0.02

The simulation results demonstrate the reliability and applicability of the derived expressions for representing the speed–time curve of a directly started IM under a gravitational load. Additionally, there is a high degree of consistency between the proposed analytical solutions and the results obtained from NTDC simulations (MATLAB/Simulink). This confirms the accuracy of modeling the dynamic behaviour of the IM under a gravitational load in real maritime operational conditions.

Figure 5 shows the speed-time and torque-time characteristics of an IM under gravitational load, comparing the results obtained from the Kloss equation with the MATLAB/Simulink simulation results. Subfigure 5a shows the speed-time curve and demonstrates a good match between the characteristics obtained using the analytical time expression (16), which employs the Kloss equation for electromagnetic torque, and the results from the MATLAB/Simulink simulations. There is a perfect alignment of the speed-time characteristics obtained from the analytical expression with the MATLAB/Simulink simulations. Subfigure 5b depicts the torque-time characteristics. It also shows a good match between the torque-time characteristics obtained using the Kloss equation and the MATLAB/Simulink simulations. The electromagnetic torque obtained from the Kloss equation exhibits a gradual increase, reaching a maximum, then stabilizing at the steady-state torque value. In contrast, the torque-time characteristics obtained from the MATLAB/Simulink simulations display an oscillatory nature, which is a consequence of the machine's dynamic operation. This oscillatory nature of the torque is directly due to the transient processes occurring during the machine's operation. Despite these oscillations in the transient period, both methods converge to the same torque values.

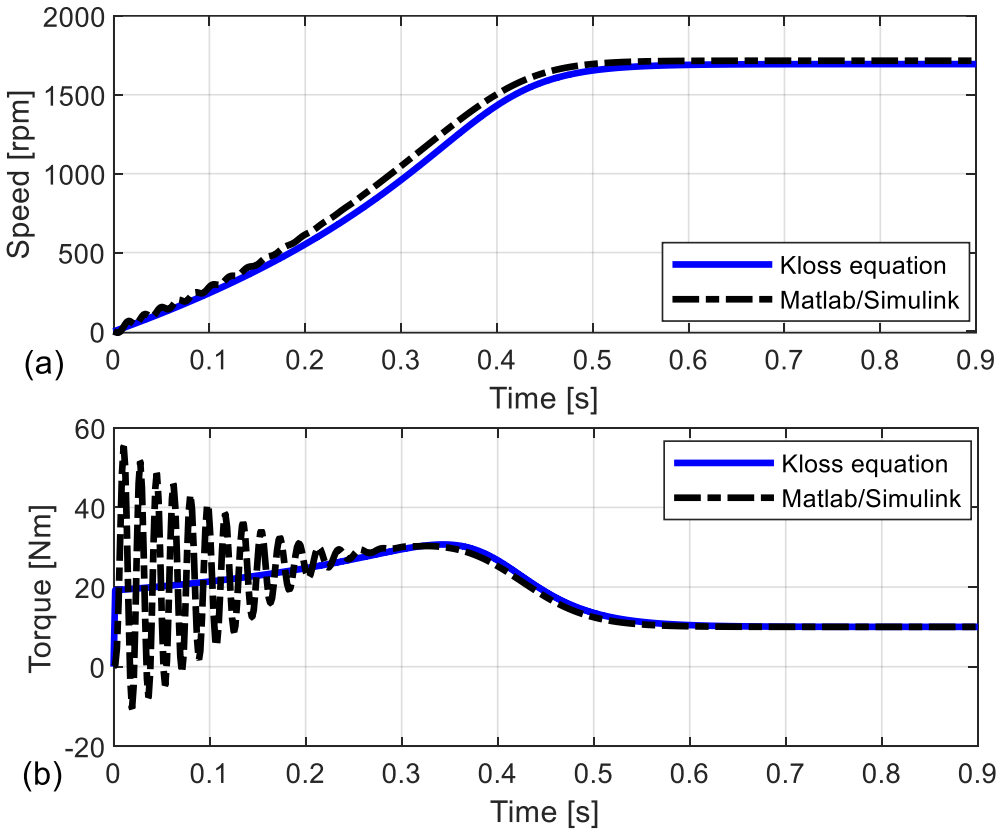

Fig. 5 Speed-time and torque-time characteristics of an IM under gravitational load for U = 300 V, B = 10 Nm, $J = 2J_n$

The speed-time profiles shown in Figures 6, 7, 8 and 9 are obtained using the analytical expression for the start-up time given in equation (16). The start-up time, given as a function of slip (s), is calculated for various speeds by discretizing the slip from $s = 1$ (standstill condition) to $s \approx 0$ (near synchronous speed) with a small step size Δs. For each discrete slip value, the corresponding time is calculated and accumulated to form the overall speed-time characteristic.

In subsequent simulations, several values of the gravitational load coefficient were selected that are lower than the nominal torque load. Subfigure 6a displays the dynamic behaviour of an IM in a simulation environment at a voltage of 450 V and a gravitational load coefficient of B = 10 Nm. This simulation

demonstrated a high consistency between the proposed models and the simulation results obtained using MATLAB/Simulink, particularly in terms of the speed at which the machine reaches a steady state. In the initial phase of the start-up, it is observed that the IM in MATLAB/Simulink exhibits mild oscillations. However, the models based on Thévenin's theorem and Kloss's equation show close alignment. Moreover, the results obtained from MATLAB/Simulink in the steady state exhibit very good consistency with Thévenin's model, indicating a robust validation of the proposed model.

Also shown in Figure 6 are the errors of the proposed models compared to the MATLAB/Simulink model for an IM with the values U = 450 V, B = 10 Nm, $J = J_n$. Subfigure 6b presents the absolute error, while subfigure 6c presents the relative error. It is evident that the proposed models closely follow the reference curve of the MATLAB/Simulink model, with some deviations during motor acceleration. The absolute error indicates the maximum deviations during acceleration, while the errors decrease as the motor reaches its steady operating speed. The relative error provides additional insight into the accuracy of the models by highlighting the percentage deviation from the reference model throughout the acceleration period. In addition to the visual representation of both absolute and relative errors, the total RMS error was calculated to quantify the accuracy of the proposed models. The RMS error for the Thévenin model is 43.41 rpm, while for the Kloss model, it is 45.97 rpm. These results confirm that both models have an acceptable deviation compared to the MATLAB/Simulink model.

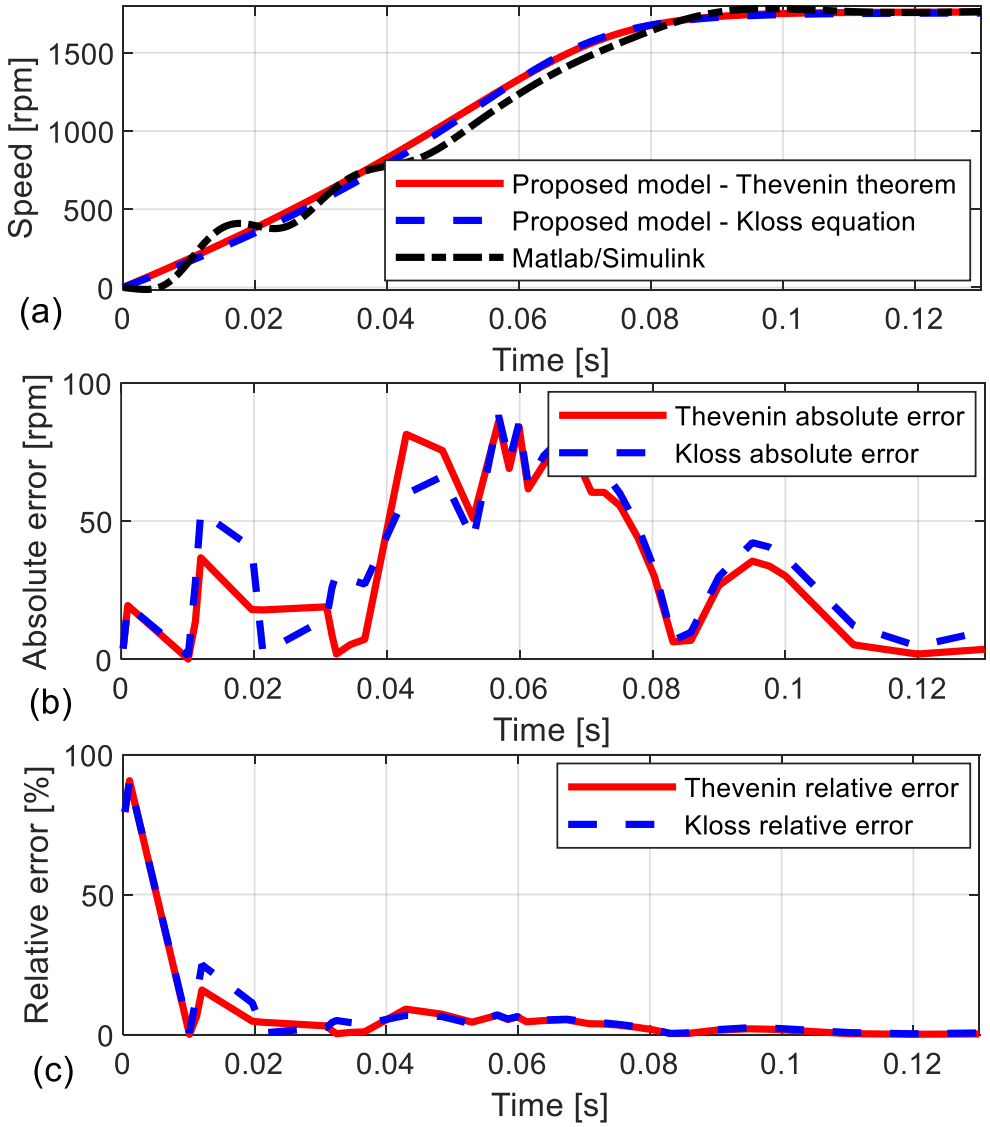

Fig. 6 Simulation results for IM at U = 450 V, B = 10 Nm, $J = J_n$; (a) Speed-time curve; (b) Absolute error; (c) Relative error

Furthermore, tests of the derived expressions with variations in the moment of inertia IM were conducted. It was shown that an increase in the moment of inertia results in longer start-up times, as illustrated in Figure 7. For smaller moments of inertia, excellent alignment of the proposed models with the models in the MATLAB/Simulink environment was recorded. In the zoomed-in view on Figure 7a, which focuses on the initial response between 0 and 0.15 seconds, slight deviations between the MATLAB/Simulink models and the models using Thévenin's expression for torque and Kloss's equation were observed. The zoomed-in view from Figure 7b shows that Thévenin's model is almost perfectly aligned with the results from MATLAB/Simulink, demonstrating very good agreement as the motor speed approaches 1776 rpm.

Figure 8 shows the results of the simulation at a supply voltage of 450 V, showing the impact of different gravitational load coefficients. Higher gravitational load coefficients result in a decrease in motor speed, indicating a slowdown in operation. The initial phase, up to 0.09 seconds, shows oscillations in the results obtained from MATLAB/Simulink. From the zoomed-in view on Figure 8a, an excellent match between the proposed Thévenin model and MATLAB/Simulink is evident. The zoomed-in view from Figure 8b, focused on the steady state, also demonstrates good correspondence between Thévenin's model and MATLAB/Simulink, confirming the effectiveness of the proposed model under various load conditions.

The results of the simulation at a gravitational coefficient of B=10 Nm and different supply voltages of 575 V, 450 V and 350 V are shown in Figure 9. The simulations indicate that lower supply voltages lead to slower acceleration of the IM. From the zoomed-in view on Figure 9a, it is evident that Thévenin's model fairly well follows the curve from MATLAB/Simulink, while Kloss's model shows deviations. The zoomed-in view from Figure 9b, focused on the steady state at the reduced voltage of 350 V, reveals discrepancies between Thévenin's and Kloss's models compared to the results from MATLAB/Simulink.

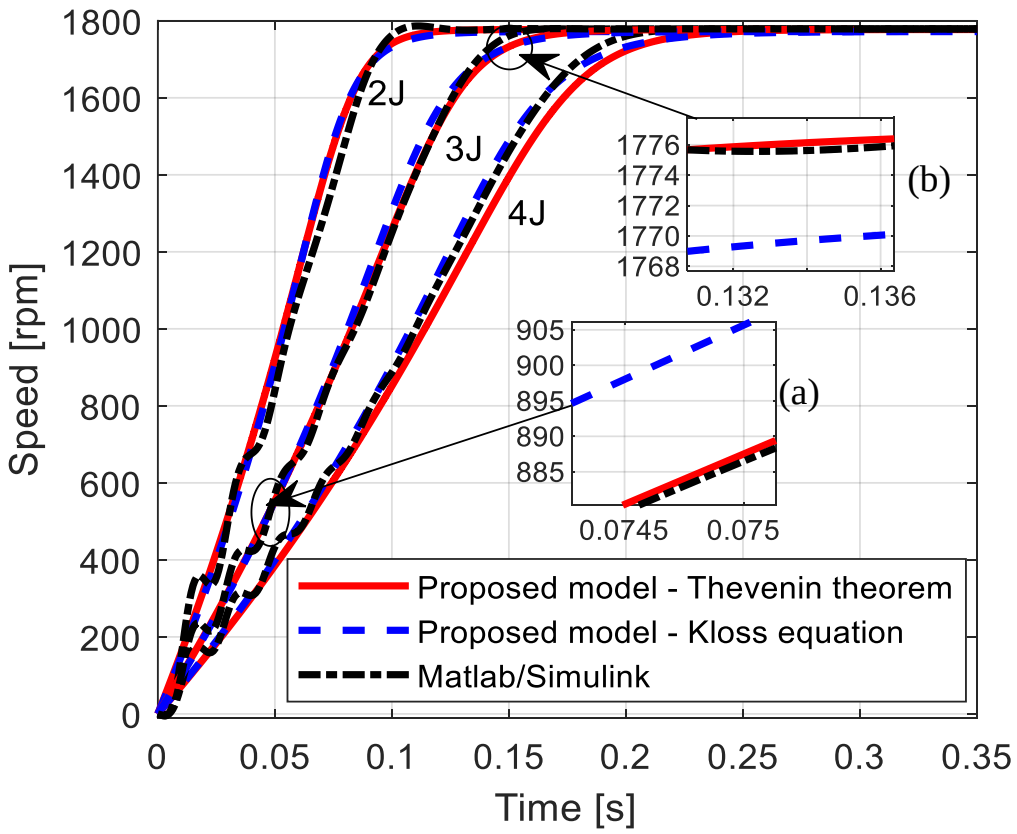

Fig. 7 Simulation results for IM at $U = U_n$, B = 10 Nm

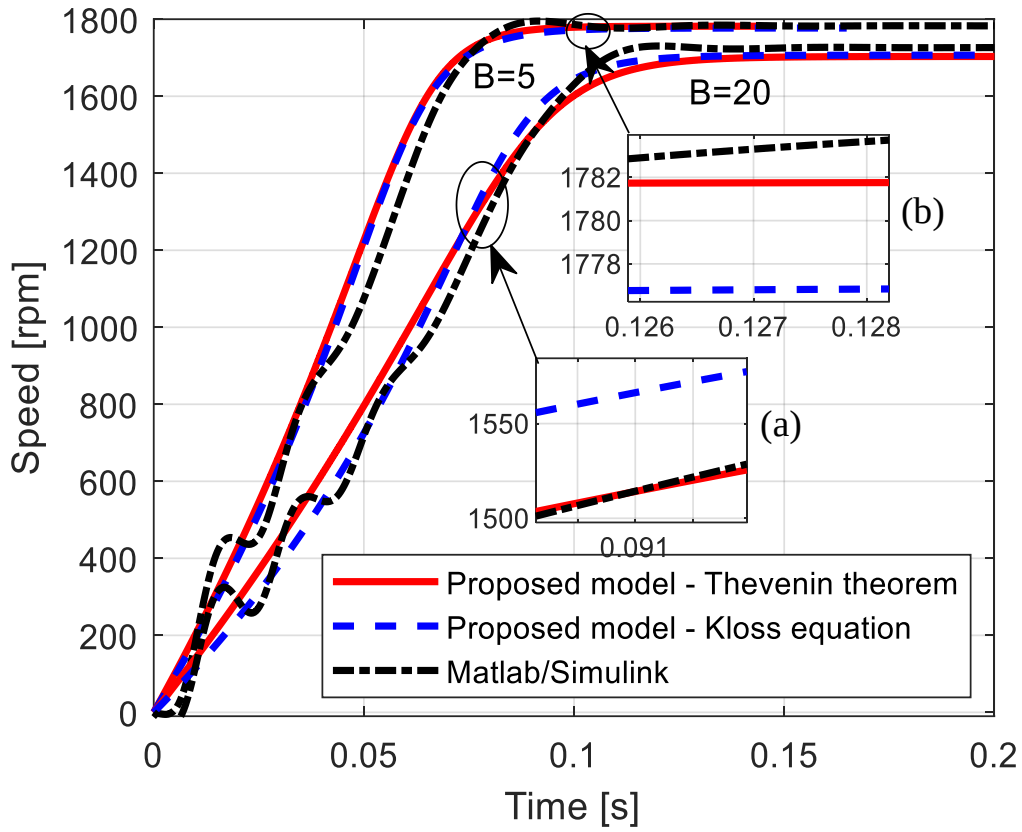

Fig. 8 Simulation results for IM at U = 450 V, $J = J_n$

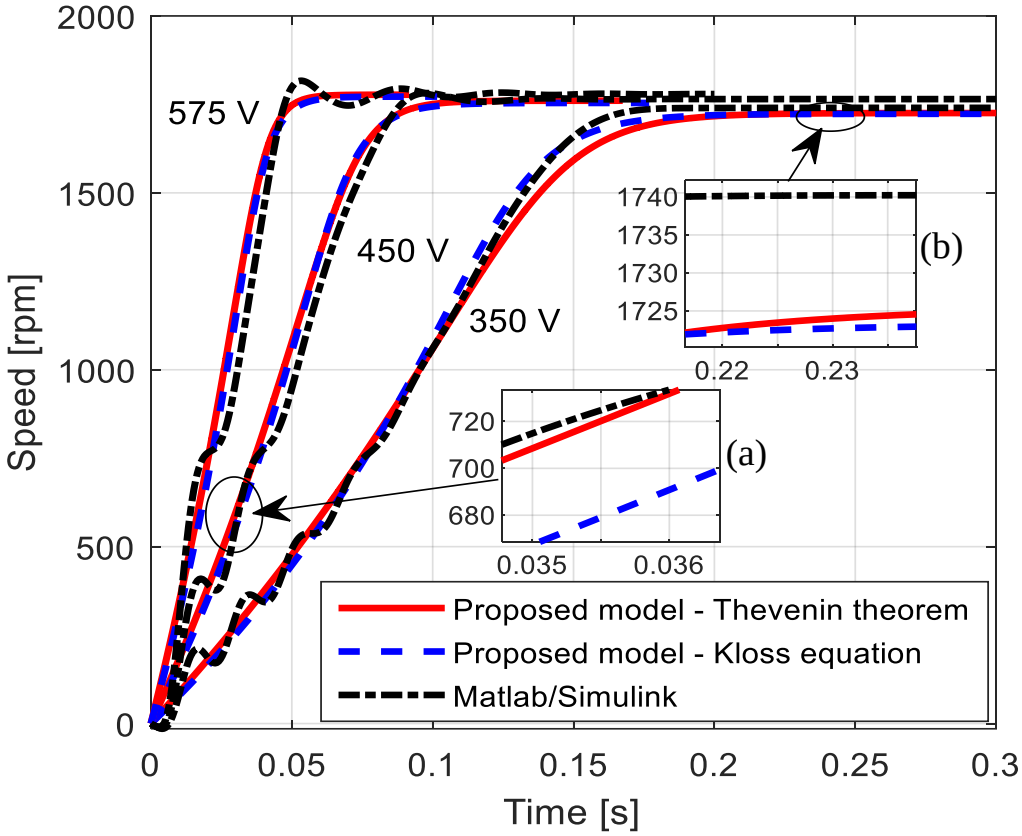

Fig. 9 Simulation results for IM at B = 10 Nm, $J = J_n$

The execution times for obtaining the speed–time characteristics using analytical models and simulations in the MATLAB/Simulink environment for various scenarios are shown in Table 2. The execution

times for MATLAB/Simulink simulations are typically around 2.5 seconds, while analytical models, such as the Thévenin and Kloss models, require between 0.25 and 0.35 seconds. In the context of smaller machines, this difference in execution time may not be critical, as both times are relatively short. However, for more complex models and larger machines, where moments of inertia are greater and supply voltage is lower, the execution time for MATLAB/Simulink simulations can be significantly longer. This highlights the additional advantage of analytical models, which are superior in terms of execution time compared to the NTDC methods used by MATLAB/Simulink. Analytical models not only offer faster processing times but also do not require specialized licensed software like MATLAB/Simulink, thereby further reducing costs.

Table 2 Execution time of the proposed analytical models and MATLAB/Simulink simulations

U **[V]**	***J*** **[kgm^2]**	***B*** **[Nm]**	***Execution time in*** **[s]** ***Kloss model***	***Execution time in*** **[s]** ***Thévenin model***	***Execution time in*** **[s]** ***MATLAB/Simulink***
450	J_n	10	0.28	0.26	2.72
575	$2J_n$	10	0.31	0.24	2.53
575	$3J_n$	10	0.35	0.25	2.69
575	$4J_n$	10	0.27	0.25	2.74
450	J_n	5	0.26	0.24	2.60
450	J_n	20	0.24	0.25	2.32
575	J_n	10	0.26	0.24	2.39
450	J_n	10	0.3	0.25	2.32
350	J_n	10	0.3	0.26	2.21

6. Experimental results

In this section, experimental investigation results are presented for the proposed mathematical expressions describing the speed–time characteristics. The validation was performed under laboratory conditions using the Lucas-Nülle test bench shown in Figure 10. This bench is equipped with a servo brake that precisely adjusts the gravitational load used to load the directly started IM. The parameters of the IM were obtained using short-circuit and no-load test methods, as detailed in paper [34], and the parameters are given in Table 3. Using the ActiveServo software, the machine was controlled and measurements were carried out with exceptional accuracy in real-time data acquisition.

The measurement results for the gravitational load coefficient B=1 Nm are visually presented in Figure 11, while the results for B=1.5 Nm are shown in Figure 12. In observing the proposed results, at high speed, a very high level of agreement between the experimentally obtained and simulated results is evident. The discrepancy between the estimated speed values and the measured speed at the start of the IM is due to the dynamics of the machine and the characteristics of the IM model. For example, the model does not consider the parameter dependency on slip or the friction moment in the bearings. This indicates the high reliability and robustness of the derived mathematical expressions and dynamic modeling of the IM.

Table 3 Parameters of the IM used for the experiment

IM parameters [34]	***Value***
P_n [W]	300
U [V]	380
f [Hz]	50
R_1 [Ω]	21.70
R_2 [Ω]	19.67
X_1 [Ω]	25.79
X_2 [Ω]	20.26
X_m [Ω]	333.7
J [Ω]	0.00175

Fig. 10 The test bench on which the proposed expressions were validated

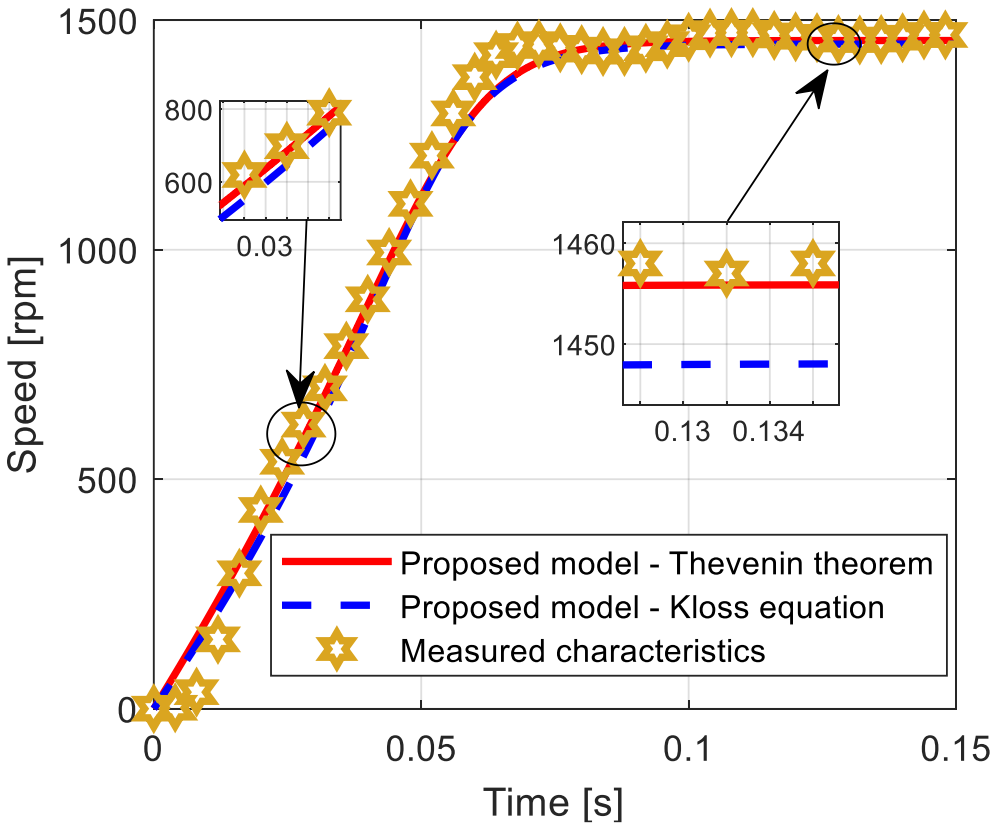

Fig. 11 Experimental results for B = 1 Nm

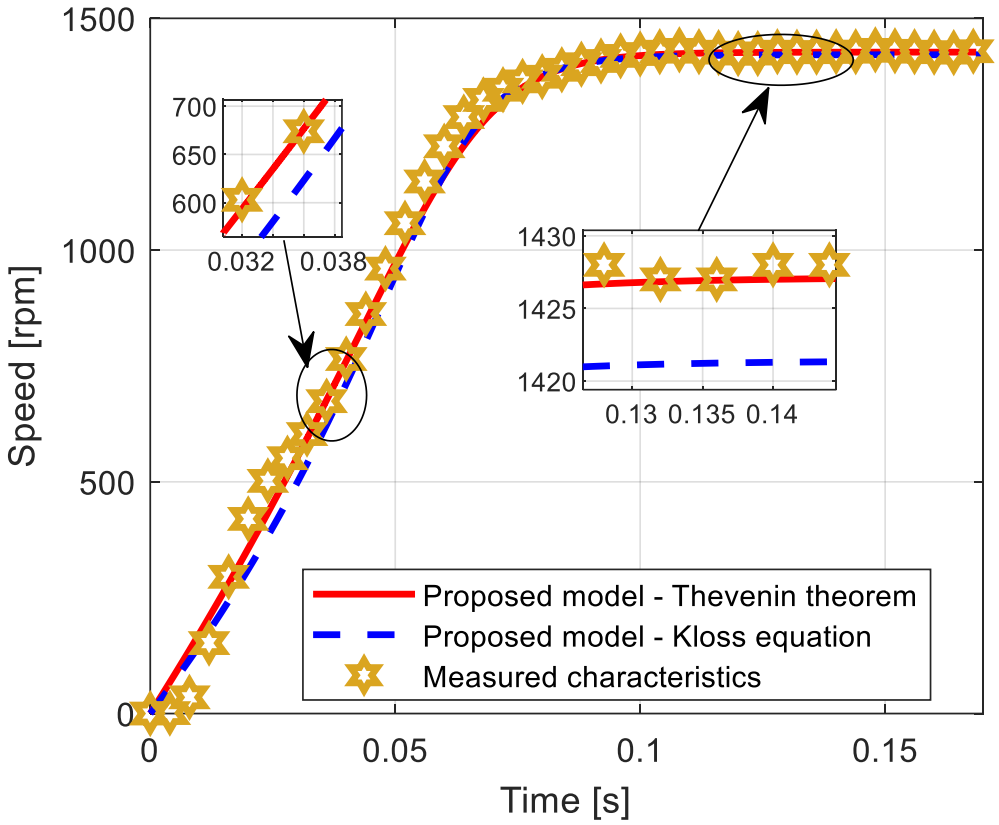

Fig. 12 Experimental results for B = 1.5 Nm

7. Conclusion

On ships, various types of auxiliary machinery are present, affecting the operation of the IMs. One of the more commonly present load characteristics of the IM on a ship is gravitational. Consequently, this paper is the first in the field to tackle the representation of the initiation time for an IM burdened with a gravitational type of load.

The paper provides novel and original mathematical equations for representing the speed–time curve of a directly started IM under a gravitational load. These mathematical expressions are derived without any assumptions. The first mathematical approach is derived from the expression for torque in Thévenin's equivalent circuit, while the second is derived from Kloss's formula for torque. Simulations of these models were tested in various operating scenarios, with results compared to those obtained using NTDC methods (MATLAB/Simulink). Moreover, experimental testing of the proposed equations was carried out under laboratory conditions on a 300 W IM, which showed an exceptional matching of the results.

The practical significance of these analytical formulas is substantial. Both models provide analytical expressions for the speed–time characteristics of a directly started IM under a gravitational type of load, which is commonly found on ships. These formulas enable accurate adjustment of protective devices and evaluation of the quality of electrical energy in the ship's power system. This ensures efficient energy management and enhances the reliability of marine operations. Such analytical expressions are useful for engineers designing marine power systems.

Future research will be directed at obtaining the inverse time-speed characteristics of directly started IMs and the influence of various types of ship auxiliary machinery on the above characteristics of the IM. Variables neglected in the modeling, such as variations in the parameters of the IM equivalent circuit with the impact of temperature and slip, will be considered in future research. Also, future research will focus on comparing the speed and time characteristics of IMs with different types of loads, and detailed analyses of the impact of different types of loads on machine characteristics.

8. Appendix

```
% Calculated UT
% Calculated RT
% Calculated XT
% Calculated Mbr
% Calculated sbr

A=J*ws;
B=J*ws*spr^2;
C=B1;
D=2*Mpr*spr;
E=B1*spr^2;
A2=A/C;
B2=B/A;
D2=D/C;
E2=E/C;
F2=B2-E2;
characteristic = [1 -D2 E2];
roots = roots([1 -D2 E2]);
real_indices = find(imag(roots) == 0);
real_roots = roots(real_indices);
sa = real_roots(real_indices(1));
sb = real_roots(real_indices(2));
matrix = [1 1; -sb -sa];
outside = [D2; F2];
solution = inv(matrix) * outside;
k1 = solution(1);
k2 = solution(2);
```

REFERENCES

[1] Paul, D., 2020. A history of electric ship propulsion systems [History]. *IEEE Industry Applications Magazine*, 26(6), 9–19. https://doi.org/10.1109/MIAS.2020.3014837

[2] Sree Krishna Prabu, C., Nagarajan, V., Sha, O. P., 2020. Study on the Lightship Characteristics of Merchant Ships. *Brodogradnja*, 71(3), 37–70. https://doi.org/10.21278/brod71304

[3] Hall, D.T., 2014. Practical Marine Electrical Knowledge, 3rd Edition. *Witherby Seamanship*, Livingston, UK.

[4] Zalacko, R., Zöldy, M., Győző, S., 2021. Comparison of Alternative Propulsion Systems – a Case Study of a Passenger Ship Used in Public Transport. *Brodogradnja*, 72(2), 1–18. https://doi.org/10.21278/brod72201

[5] Wang, Y., Lipo, T. A., Pan, D., 2011. Robust Operation of Double-Output AC Machine Drive. *8th International Conference on Power Electronics – ECCE Asia*, 30 May- 3 June, Jeju, South Korea 140–144. https://doi.org/10.1109/ICPE.2011.5944562

[6] Narayanasamy, M., Sukhi, Y., 2023. Rotor Short-Circuited Start-up Strategy for a Doubly Fed Induction Machine-Fed Large-Rated Variable-Speed Pumped Storage Unit Operating in Pumping Mode. *Journal of Power Electronics*, 1–12. https://doi.org/10.1007/s43236-023-00662-8

[7] Sano, M., 2023. Mathematical Model and Simulation of Cooperative Manoeuvres among a Ship and Tugboats. *Brodogradnja*, 74(2), 127–148. https://doi.org/10.21278/brod74207

[8] Dai, K., Li, Y., 2021. Experimental and Numerical Investigation on Maneuvering Performance of Small Waterplane Area Twin Hull. *Brodogradnja*, 72(2), 93–114. https://doi.org/10.21278/brod72206

[9] Kanevskii, G., Klubnichkin, A., Sazonov, K., 2020. Propulsion Performance Prediction Method for Multi Shaft Vessels. *Brodogradnja*, 71(3), 27–36. https://doi.org/10.21278/brod71303

[10] Sulligoi, G., Vicenzutti, A., Menis, R., 2016. All-Electric Ship Design: From Electrical Propulsion to Integrated Electrical and Electronic Power Systems. *IEEE Transactions on transportation electrification*, 2(4), 507–521. https://doi.org/10.1109/TTE.2016.2598078

[11] Tarasiuk, T., Jayasinghe, S. G., Gorniak, M., Pilat, A., Shagar, V., Liu, W., Guerrero, J. M., 2021. Review of Power Quality Issues in Maritime Microgrids. *IEEE Access*, 9, 81798–81817. https://doi.org/10.1109/ACCESS.2021.3086000

[12] Mukund, R. P., 2012. Shipboard Electrical Power Systems. *CRC Press*, Boca Raton, FL, USA.

[13] Kulkarni, S., Santoso, S., 2009. Impact of Pulse Loads on Electric Ship Power System: With and without Flywheel Energy Storage Systems. *2009 IEEE Electric Ship Technologies Symposium*, 20-22 April, Baltimore, Maryland, USA, 568–573. https://doi.org/10.1109/ESTS.2009.4906568

[14] Giulivo, D., Sulligoi, G., Tessarolo, A., 2010. Electric Motors and Drives for Modern Ship Thruster Propulsion: Design and System Integration Issues. *Electrical Systems for Aircraft, Railway and Ship Propulsion*, 19-21 October, Bologna, Italy, 1–6. https://doi.org/10.1109/ESARS.2010.5665230

[15] Cergol, V., Vidmar, P., 2015. An Enhanced Equation for Vibration Prediction of New Types of Ships. *Brodogradnja*, 66(3), 91–117.

[16] Reusser, C. A., Young, H. A., Osses, J. R. P., Perez, M. A., Simmonds, O. J., 2020. Power Electronics and Drives: Applications to Modern Ship Propulsion Systems. *IEEE Industrial Electronics Magazine*, 14(4), 106–122. https://doi.org/10.1109/MIE.2020.3002493

[17] Bosich, D., Filippo, M., Giulivo, D., Sulligoi, G., and Tessarolo, A., 2012. Thruster motor start-up transient in an all-electric cruise-liner: Numerical simulation and experimental assessment. *Electrical Systems for Aircraft, Railway and Ship Propulsion*, 16-18 October, Bologna, Italy, 1–5. https://doi.org/10.1109/ESARS.2012.6387447

[18] Gnaciński, P., Tarasiuk, T., Mindykowski, J., Pepliński, M., Górniak, M., Hallmann, D., Piłlat, A., 2020. Power Quality and Energy-Efficient Operation of Marine Induction Motors, *IEEE Access*, 8, 152193–152203. https://doi.org/10.1109/ACCESS.2020.3017133

[19] Cvrk, S., and Ilijević, D., 2020. Application of Diagnostics as a Basis of Condition Based Maintenance of the Marine Propulsion Diesel Engine. *Brodogradnja*, 71(3), 119–134. https://doi.org/10.21278/brod71307

[20] Pillay, K., Nour, M., Yang, K. H., Datu Harun, D. N., Haw, L. K., 2009. Assessment and Comparison of Conventional Motor Starters and Modern Power Electronic Drives for Induction Motor Starting Characteristics. *2009 IEEE Symposium on Industrial Electronics & Applications*, 4-6 October, Kuala Lumpur, Malaysia, 584–589. https://doi.org/10.1109/ISIEA.2009.5356387

[21] Pallis, I. K., Georgakopoulos, I. P., Tatakis, E. C., 2014. Modern starting methods of large thrusters supplied by the power network of a ship. *International Conference on Electrical Machines (ICEM)*, Berlin, Germany, 2325–2331. https://doi.org/10.1109/ICELMACH.2014.6960510

[22] Hughes, A., 2006. Electric Motors and Drives: Fundamentals, Types and Applications, 3rd Edition. Newnes.

[23] Badr, M. A., Abdel-Halim, M. A., Alolah, A. I., 1996. A Nonconventional Method for Fast Starting of Three Phase Wound-Rotor Induction Motors. *IEEE Transactions on Energy Conversion*, 11(4), 701–707. https://doi.org/10.1109/60.556366

[24] Lin, W.-M., Su, T.-J., Wu, R.-C., 2012. Parameter Identification of Induction Machine With a Starting No-Load Low-Voltage Test. *IEEE Transactions on Industrial Electronics*, 59, 352–360. https://doi.org/10.1109/TIE.2011.2148674

[25] Kucuk, S., Ajder, A., 2022. Analytical Voltage Drop Calculations during Direct on Line Motor Starting: Solutions for Industrial Plants. *Ain Shams Engineering Journal*, 13(4), https://doi.org/10.1016/j.asej.2021.101671

[26] Banerjee, A., Banerjee, A., Saikat Rana, D. P., Shubhanga, K. N., 2015. A Study of Starting Methods for an Induction Motor Using an Arbitrary Waveform Generator. *2015 International Conference on Advances in Electrical Engineering (ICAEE)*, 7-19 December, Dhaka, Bangladesh, 34–37. https://doi.org/10.1109/ICAEE.2015.7506790

[27] Aree, P., 2016. Starting time calculation of large induction motors using their manufacturer technical data. *19th International Conference on Electrical Machines and Systems (ICEMS)*, 13-16 November, Chiba, Japan, 1–5.

[28] Ćalasan, M. P., 2020. An Invertible Dependence of the Speed and Time of the Induction Machine during No-Load Direct Start-Up. *Automatika*, 61(1), 141–149. https://doi.org/10.1080/00051144.2019.1689725

[29] Automation, R., 2004. Application basic of operation of three-phase induction motors: design duty types selection dimensioning. *Power Technologies Inc*, Schenectady, 19–24.

[30] Aree, P., 2018. Precise analytical formula for starting time calculation of medium- and high-voltage induction motors under conventional starter methods. *Electrical Engineering*, 100(2), 1195–1203. https://doi.org/10.1007/s00202-017-0575-6

[31] Ćalasan, M. P., 2019. Analytical solution for no-load induction machine speed calculation during direct start-up. *International Transactions on Electrical Energy Systems*, 29(4). https://doi.org/10.1002/etep.2777

[32] Koljčević, N., Fuštić, Ž., Ćalasan, M., 2020. Analytical solution for determination of induction machine acceleration based on Kloss equation. *Serbian Journal of Electrical Engineering*, 17(2), 247–256. https://doi.org/10.2298/SJEE2002247K

[33] Ćalasan, M., Alqarni, M., Rosić, M., Koljčević, N., Alamri, B., Abdel Aleem, S. H. E., 2021. A Novel Exact Analytical Solution Based on Kloss Equation towards Accurate Speed–Time Characteristics Modeling of Induction Machines during No-Load Direct Startups. *Applied Sciences*, 11(11), 5102. https://doi.org/10.3390/app11115102

[34] Knežević, I., Ćalasan, M., Dlabač, T., 2023. Novel Analytical Approaches for Induction Machine Direct Start-up Speed–Time Curve Modeling under Fan Load. *Electrical Engineering*, 1–14. https://doi.org/10.1007/s00202-023-02039-3

[35] Mrdović, L., Pudar, N., Knežević, I., ćalasan, M., Cvrk, S., Dlabač, T., 2023. Improvement of Education in the Field of Marine Engineering at the Faculty of Maritime Studies Kotor. *10th International Conference on Electrical, Electronic and Computing Engineering (IcETRAN 2023)*, 5-8 June, East Sarajevo, Bosnia and Herzegovina. https://doi.org/10.1109/IcETRAN59631.2023.10192127

[36] Limpaecher, R., 2000. Novel converters for electric ship propulsion system and shipboard power distribution. *Conference Record of the 2000 Twenty-Fourth International Power Modulator Symposium*, 26-29 June, Norfolk, VA, USA, 89–96. https://doi.org/10.1109/MODSYM.2000.896172

[37] Giuffrida, M., 2013. Electrical Plants and Electric Propulsion on Ships. First Edition, Lulu.com, Switzerland.

[38] Molland, A. F., 2008. Chapter 6 – Marine engines and auxiliary machinery. *The Maritime Engineering Reference Book*. Oxford: Butterworth-Heinemann, 344–482.

[39] McGeorge, H. D., 1993. Marine Electrical Equipment and Practice, Second Edition. *Butterworth-Heinemann Ltd*, 130–135. https://doi.org/10.1016/B978-0-08-093812-7.50013-8